

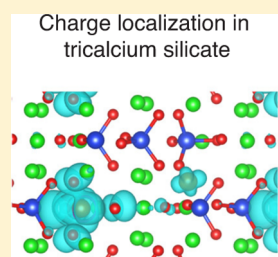
# Predicting Electronic Structure in Tricalcium Silicate Phases with Impurities Using First-Principles

Kayahan Saritas,\* Can Ataca, and Jeffrey C. Grossman\*

Department of Materials Science and Engineering, Massachusetts Institute of Technology, Cambridge, Massachusetts 02139, United States

## Supporting Information

**ABSTRACT:** Tricalcium silicate ( $\text{Ca}_3\text{SiO}_5$ ) is heavily used in industry as it is the most predominant constituent in Portland cement clinkers. In this work, using ab-initio calculations, we assess the ability of a large selection of substitutions to modify the electronic structure in the M3 polymorph of tricalcium silicate. We demonstrate the relation between electronic structure, hybridization of the impurity orbitals, and charge transfer from impurity atoms to the bulk material. Our work suggests that charge localization upon introducing impurities can passivate the reactive sites and several such substitutions are identified.



## INTRODUCTION

Tricalcium silicate ( $\text{Ca}_3\text{SiO}_5$  or  $\text{C}_3\text{S}$ ) is considered to be the most predominant compound in ordinary Portland cement clinkers, at  $\sim 50$ – $70$  wt %.<sup>1,2</sup>  $\text{C}_3\text{S}$  is usually chemically modified upon substituting with impurities, forming a solid solution which is called alite. The amount and content of the impurities in  $\text{C}_3\text{S}$  can determine the physical and chemical properties of the resulting cement such as hydration reactivity,<sup>3–5</sup> polymorphism,<sup>1</sup> corrosion resistance,<sup>2</sup> and elastic properties.<sup>6</sup> From the energy consumption perspective, among other phases in cement, producing  $\text{C}_3\text{S}$  requires the highest processing temperature, which accounts for roughly 5% of global  $\text{CO}_2$  emissions.<sup>7</sup> As it is also the most reactive, a substantial amount of  $\text{C}_3\text{S}$  is necessary to have satisfactory early setting properties.<sup>1,2</sup> Much effort has been spent developing cement using industrial waste products that can provide the same reactivity properties as ordinary Portland cement clinkers, although these products introduce a wide range of impurities to different phases in the cement.<sup>8</sup> Although several impurities have been found to decrease the reactivity of  $\text{C}_3\text{S}$ , thus decreasing performance even when used in trace amounts, a comprehensive understanding of the chemical behavior of different impurities in  $\text{C}_3\text{S}$  is still lacking.<sup>9</sup> Experimental studies in the field mostly focus on the effect of different impurities by examining their volatility during production as a measure of their incorporation into different phases. However, probing different phases in cement with such impurities can be challenging, and conflicting results can be open to interpretation due to the complexity of the material itself.<sup>10</sup>

In this paper, we use quantum mechanical computational methods to analyze the structural and electronic properties of  $\text{C}_3\text{S}$ . We examine the changes in the electronic structure, upon introduction of a wide range of impurities. Such properties of different substitutions in the dicalcium silicate ( $\text{Ca}_2\text{SiO}_4$  or  $\text{C}_2\text{S}$ ) structure including a preliminary comparison between alite and belite (second most compound in portland cement)

structures for the Mg, Al, and Fe substitutions has already been examined by Durgun et al.<sup>3</sup> In this work we build upon this methodology and extend the range of impurities investigated in alite substitution. We additionally support these hypotheses with partial density of states analyses and suggest a relation between the electronic structure of some impurities and their atomic radii.

## COMPUTATIONAL DETAILS

We performed calculations using density functional theory (DFT),<sup>11,12</sup> using the projector augmented plane wave method<sup>13</sup> (PAW) implemented in the VASP<sup>14,15</sup> package. The Perdew–Burke–Ernzerhof (PBE) generalized gradient approximation<sup>16</sup> is used to calculate the exchange correlation energy with a 500 eV kinetic energy cutoff for the plane wave basis set. A  $4 \times 4 \times 4$  k-point grid centered at the gamma point is chosen for sampling the Brillouin zone, which was sufficient to converge energies to within  $10^{-5}$  eV per atom in the unit cell. For supercell calculations the density of k-points was scaled accordingly. Structural minimization using a conjugate gradient approach was carried out until the maximum force component on each atom was smaller than  $10^{-3}$  eV/Å. For atomic basin charge analysis of the relevant structures, we use the Bader charge analysis.<sup>17,18</sup>

## RESULTS AND DISCUSSION

In order to examine the effect of impurities on the  $\text{C}_3\text{S}$  phase, we examine its monoclinic M3 ( $\text{M3-C}_3\text{S}$ ) polymorph, which is considered to be the most frequently observed in industrial applications, constituting 50–70%.<sup>1</sup> In this unit cell there are 18 Ca, 6 Si, and 30 O atoms<sup>19</sup> (see Figure S1 in the Supporting

Received: October 21, 2014

Revised: January 29, 2015

Published: January 30, 2015



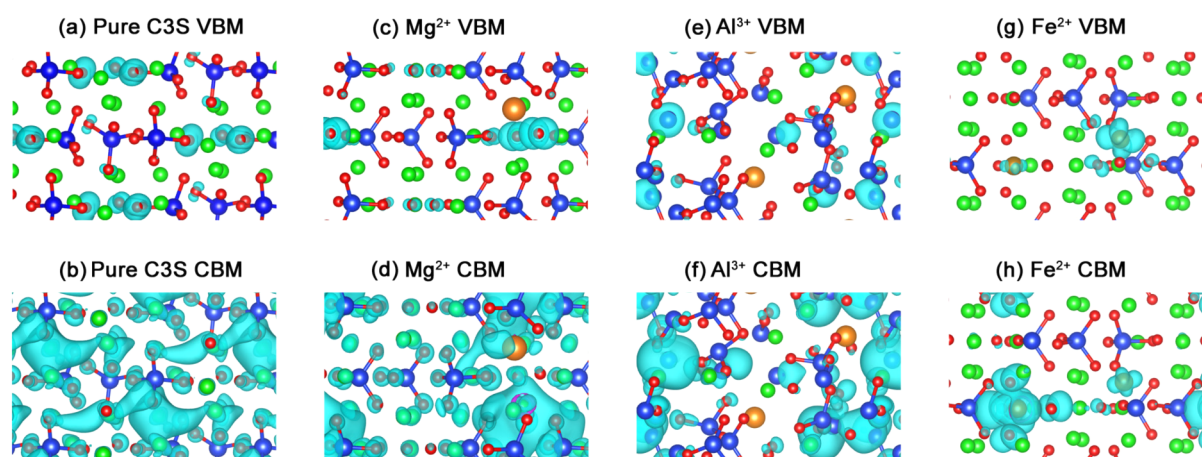


**Figure 1.** Band decomposed charge densities at the valence band maximum and conduction band minimum,  $\rho_{\text{VBM}}$  and  $\rho_{\text{CBM}}$ , of M3-C<sub>3</sub>S for (a),(b) pure; (c),(d) Mg; (e),(f) Al; and (g),(h) Fe doped structures. Green spheres indicate Ca; blue spheres indicate Si; red spheres indicate O; and orange spheres indicate respective impurity atoms in each figure.<sup>23</sup>

Information). Twenty-four oxygen atoms in the unit cell are bonded to neighboring silicons in a tetrahedral orientation with bond distances of 1.64–1.67 Å, while the remaining six oxygens are ionically bonded to calcium atoms in octahedral coordination with significantly longer bond distances of 2.33–2.48 Å. We use the experimental unit cell in ref 19 with lattice parameters  $a = 12.22$  Å,  $b = 7.08$  Å,  $c = 9.30$  Å, and  $\beta = 114.93^\circ$  as the starting unit cell for the ionic relaxation calculations using DFT. Our computed lattice parameters yield  $a = 12.21$  Å,  $b = 7.11$  Å,  $c = 9.23$  Å, and  $\beta = 116.08^\circ$ , in good agreement with experimental data.

Within the framework of DFT, the Fukui function has been generalized from frontier molecular orbital theory of chemical reactivity to the charge density description for bulk systems.<sup>20</sup> Under a constant external potential,  $\nu(r)$ , the Fukui function  $f(r)$  can be described as the change in the electron density  $\rho(r)$  at each point  $r$  with respect to the differential change in the total number of electrons,  $N$ , in the system:  $f(r) = (\partial\rho(r)/\partial N)_{\nu(r)}$ .<sup>21</sup> Because of the well-known derivative discontinuity problem,<sup>22</sup> the Fukui function has one-sided limits when it is approached from left and right at constant number of total electrons. Therefore, electrophilic attack, which causes an electron decrease in the system, is defined as  $f^-(r) = (\partial\rho(r)/\partial N)_{\nu(r)}^-$ , and nucleophilic attack which causes an electron increase in the system is defined as  $f^+(r) = (\partial\rho(r)/\partial N)_{\nu(r)}^+$ . For bulk systems, using the finite difference method, these quantities can be approximated as the following:  $f^-(r) \approx \rho(r)_{\text{VBM}}$  and  $f^+(r) \approx \rho(r)_{\text{CBM}}$ , where VBM stands for valence band maximum and CBM is conduction band minimum.<sup>20</sup>

It has been shown that the Fukui function can be used to identify charge localized regions, which can be used to tailor reactive sites in a system.<sup>20,22,24</sup> In a similar fashion to frontier molecular orbital theory, regions where the value of the Fukui function is larger will more likely undergo an external chemical attack and be more reactive than the rest of the system. The spread of the Fukui function can also provide useful information regarding the degree of localization for chemical activity in such sites. It has been reported that the presence of ionically bonded oxygens in C<sub>3</sub>S yields a higher reactivity compared to C<sub>2</sub>S, due to the fact that there are no ionically bonded oxygen atoms C<sub>2</sub>S and that covalently bonded silicate tetrahedra in both systems do not influence reactivity.<sup>3,4</sup> With these findings we can postulate that the reactivity of C<sub>3</sub>S could

be enhanced by concentrating  $\rho_{\text{CBM}}$  and  $\rho_{\text{VBM}}$  on the ionic components, Ca<sup>2+</sup> and O<sup>2-</sup>, respectively. However, if the substitution induces  $\rho_{\text{CBM}}$  and  $\rho_{\text{VBM}}$  to concentrate mostly on impurity atoms, this will localize the reactive sites on the impurities and could affect hydration kinetics adversely. Therefore, identifying the impurity atoms which cause heavy localization on their substitution sites may be useful to determine impurity atoms that will suppress the reactivity of alite. We note that the electronic state structure picture presented here, while useful for gaining understanding of the changes in reactive sites upon chemical substitution, may not correlate directly with the hydration dynamics of the same surface. For that, dynamical effects that include both chemical changes as well as possible surface topological changes must be taken into account, and will be the subject of future work.

We examine several doped C<sub>3</sub>S structures with the impurities Mg, Al, and Fe, since their oxides are the most prominently found foreign oxides in calcium silicate phases.<sup>1</sup> It is reported that the maximum amounts of impurities that can be contained in M3-C<sub>3</sub>S vary with the type of impurity.<sup>1</sup> However, we note that the aim of this study is not to model alite under realistic impurity concentrations but rather to identify how different impurities modify the charge density at the substitution sites and how this may correspondingly affect the reactivity of the alite phase. Towards this end, we perform direct site substitutions while preserving charge neutrality for all unique substitution cases to find the minimum energy configurations. Previous work on bulk C<sub>3</sub>S phases using classical force fields showed that although the substitution energy varies with site it does not follow a clear trend with substitute atom distance.<sup>4</sup> However, it is not possible to identify changes in the charge density using classical molecular dynamics methods. Accordingly, using DFT, we performed impurity substitutions on the single unit cell C<sub>3</sub>S. Ca<sup>2+</sup> is substituted with Mg<sup>2+</sup> and Ca<sup>2+</sup> + Si<sup>4+</sup> with two Al<sup>3+</sup> or two Fe<sup>3+</sup> atoms. Our  $\rho_{\text{VBM}}$  and  $\rho_{\text{CBM}}$  results are shown in Figures 1(a) and 1(b) for pure C<sub>3</sub>S and, respectively, in 1(c) and 1(d) for Mg substitution, 1(e) and 1(f) for Al substitution, and finally 1(g) and 1(h) for Fe substitution. In pure C<sub>3</sub>S,  $\rho_{\text{VBM}}$  is localized over ionic oxygens, whereas  $\rho_{\text{CBM}}$  spreads almost evenly throughout the unit cell. This suggests that ionic oxygens are more likely to lose electrons compared to the rest of the system, and therefore they will undergo electrophilic attack with cations such as H<sup>+</sup>,

$\text{Na}^{2+}$ ,  $\text{Mg}^{2+}$ , and  $\text{Ca}^{2+}$ . Since  $\rho_{\text{CBM}}$  is delocalized in pure  $\text{C}_3\text{S}$ , there is no distinctive region that is more prone to nucleophilic attack such as  $\text{OH}^-$  and  $\text{SO}_4^{2-}$ . However, when the  $\text{Ca}^{2+}$  is substituted with  $\text{Mg}^{2+}$ , the spreads of both  $\rho_{\text{VBM}}$  and  $\rho_{\text{CBM}}$  decrease slightly, but  $\rho_{\text{VBM}}$  localizes around the ionic oxygens that are neighboring  $\text{Mg}^{2+}$  atoms. The effect is slightly more pronounced for  $\text{Al}^{3+}$  substitution. With only these data, it is hard to deduce how these impurities could modify the reactive sites. While the oxygens near the impurities localize the charge around them which makes them more reactive, they may also decrease the number of available reactive sites that could decrease the overall reactivity of  $\text{C}_3\text{S}$ . In the case of  $\text{Fe}^{3+}$  substitution we see stronger localization of charge density in both  $\rho_{\text{VBM}}$  and  $\rho_{\text{CBM}}$  mainly on the impurity atom, which suggests a more definite reduction for the reactivity of this site.

In addition to examining the nature of charge localization over particular sites in doped  $\text{C}_3\text{S}$  structures, we also investigate how the partial density of states (PDOS) responds to doping. With this analysis we can understand which atoms or orbitals contribute more to the total density of states (DOS) of the  $\text{C}_3\text{S}$  crystal structure near band edges and therefore would be more susceptible to lose or withdraw electrons. Figure 2 shows that

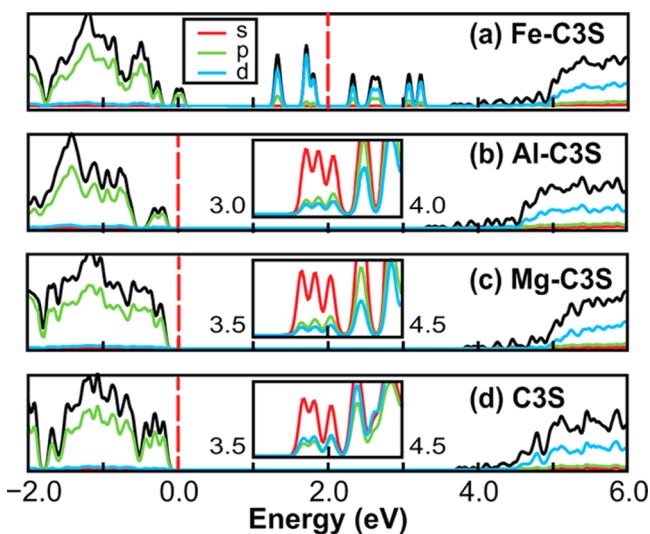


**Figure 2.** Partial density of states for a) Fe, b) Al, c) Mg-doped and the pure  $\text{C}_3\text{S}$  cases. Red, green and cyan lines indicate density of states projected on s, p and d orbitals, respectively. The insets of Figure (b), (c) and (d) show the s, p, d partial density of states 8X magnified near the conduction band. The dashed red line in each plot shows the location of Fermi energy.

the DOS for Al- and Mg-doped  $\text{C}_3\text{S}$  are similar to the pure  $\text{C}_3\text{S}$  electronic structure, but for Fe-doped  $\text{C}_3\text{S}$ , we observe a metallic-like band structure due to the large number of localized states formed mostly from Fe d-orbitals near the Fermi energy. When we look at the PDOS for Al- and Mg-doped  $\text{C}_3\text{S}$ , we observe that these two atoms slightly modify the DOS near both the conduction and valence bands. Upon substitution, Al and Mg atoms localize the charge density by hybridizing with surrounding oxygen p-orbitals. The contribution of p-orbitals to the density of states at the conduction band slightly increases, as can be seen when Figure 2(b), (c), and (d) insets are compared. This analysis reinforces our findings from the  $\rho_{\text{VBM}}$  and  $\rho_{\text{CBM}}$  profiles that as the impurities undergo stronger hybridization at the conduction band they can have a more distinctive effect on electronic structure of the reactive sites.

The reason for the modification of the PDOS may be the different charge donation properties of Ca, Mg, and Al in  $\text{C}_3\text{S}$  which change the bonding between them and the surrounding oxygens, causing accumulation of extra charge on these oxygen p-orbitals.

Further examination of the charge transfer of the impurities with respect to the pure structure can give additional insight regarding their oxidation character and localization of the charge density in the structure. Bader charge analysis over the pure M3- $\text{C}_3\text{S}$  structure shows that each Ca atom donates  $1.55 e^-$  on average to the unit cell; each Si atom donates  $3.12 e^-$ ; each tetrahedral O atom,  $\text{O}_t$ , withdraws  $1.45 e^-$ ; and each ionic O atom,  $\text{O}_i$ , withdraws  $1.54 e^-$  from the unit cell. In the case of Mg substitution, the Mg atom donates an additional  $0.18 e^-$  charge to the unit cell. This additional charge and enhancement of O p-orbitals around the CBM, as shown in Figure 2(c), can explain the slight charge localization around the Mg atom observed in Figure 1(c) and (d). For Al substitution, we have a similar finding in terms of charge localization as in the Mg case, but each Al atom donates  $0.6 e^-$  more to the system, where the reference atoms, Ca + Si, donate  $4.67 e^-$  to the structure. As indicated in Figure 1(e) and (f), in Al substitution the charge donation is larger and the induced charge localization also stronger compared to Mg substitution. In the case of Fe substitution, two Fe atoms donate  $2.49 e^-$  in total, decreasing the amount of charge transferred to the structure by  $1.09 e^-$  per atom. Combined with the PDOS analysis in Figure 2(a), we see that much of the charge has remained on the d-orbitals of Fe atoms, which can also be deduced from the shape of the charge density on Fe in Figure 1(g) and (h), leading to strongly localized charge on this impurity. Several experimental studies regarding Al substitution demonstrate either acceleration<sup>25</sup> or delay<sup>26</sup> in hydration reactivity. Similarly, conflicting results for Mg-doped alite reactivity are also found, showing either a decrease, increase, or no change in the reactivity.<sup>26–28</sup> These differences could have occurred due to differences in particle sizes, storage conditions, water to solid ratio, and grinding conditions. According to our analysis, upon Mg substitution with Ca, the electronic structure of  $\text{C}_3\text{S}$  is only slightly altered. Our findings for the Fe substitution are in a good agreement with experimental studies which have shown that Fe decreases overall alite reactivity,<sup>27,29</sup> by complete localization of the both CBM and VBM.

Since we already discussed how the electronic structure is modified when  $\text{C}_3\text{S}$  is substituted with Mg, Al, and Fe atoms, we turn our attention to different impurities incorporated into the M3- $\text{C}_3\text{S}$  unit cell. We consider the following substitutions: (1) one  $\text{Ca}^{2+}$  atom with either two +1 oxidation state atoms in a dumbbell orientation or one +2 oxidation state atom, (2) one  $\text{Ca}^{2+}$  and one  $\text{Si}^{4+}$  atom with either two +3 oxidation state atoms or group I A and group V A atoms, (3) one  $\text{Ca}^{2+}$  and one  $\text{O}^{2-}$  with group I A and group VII A atoms, (4) both tetrahedral and ionic  $\text{O}^{2-}$  with other group VI A atoms, (5) two  $\text{Si}^{4+}$  atoms with either group III A and group V A atoms or two other group IV A atoms, and (6) one  $\text{Si}^{4+}$  and one  $\text{O}^{2-}$  atom with one group III A and one group VII A atoms. In alite, ionically bonded oxygens are more susceptible to deformation than tetrahedral oxygens, and a defect balancing mechanism is reported as the reorientation of Si tetrahedra, which essentially conserves their shape and composition upon substitution.<sup>1,4</sup> Therefore, we perform oxygen substitutions only on ionic oxygen sites when more than one atom substitution is made, but nevertheless we also performed substitutions on tetrahedral

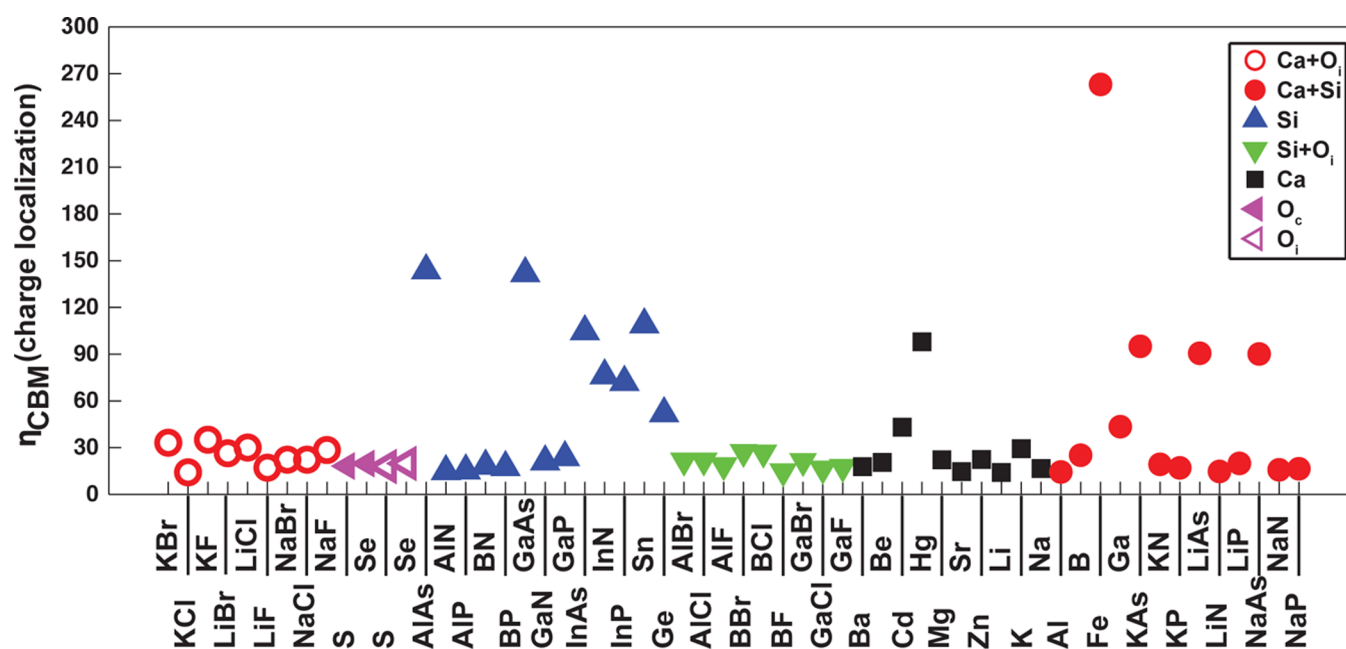


**Figure 3.** Charge localization on the conduction band minimum,  $\eta_{\text{CBM}}$ , is defined as the maximum charge density value (MCD) of the band decomposed charge density at the conduction band minimum for doped over pure  $\text{C}_3\text{S}$ :  $\eta_{\text{CBM}} = \text{MCD}_{\text{doped}}/\text{MCD}_{\text{pure}}$ .  $\eta_{\text{CBM}}$  values are shown as different impurities indicated on the  $x$ -axis are substituted for the respective atoms in pure  $\text{C}_3\text{S}$  as indicated in the upper right legend.  $\text{O}_i$  corresponds to ionic oxygen substitutions, whereas  $\text{O}_c$  corresponds to covalently bonded oxygen substitutions in pure  $\text{C}_3\text{S}$ .

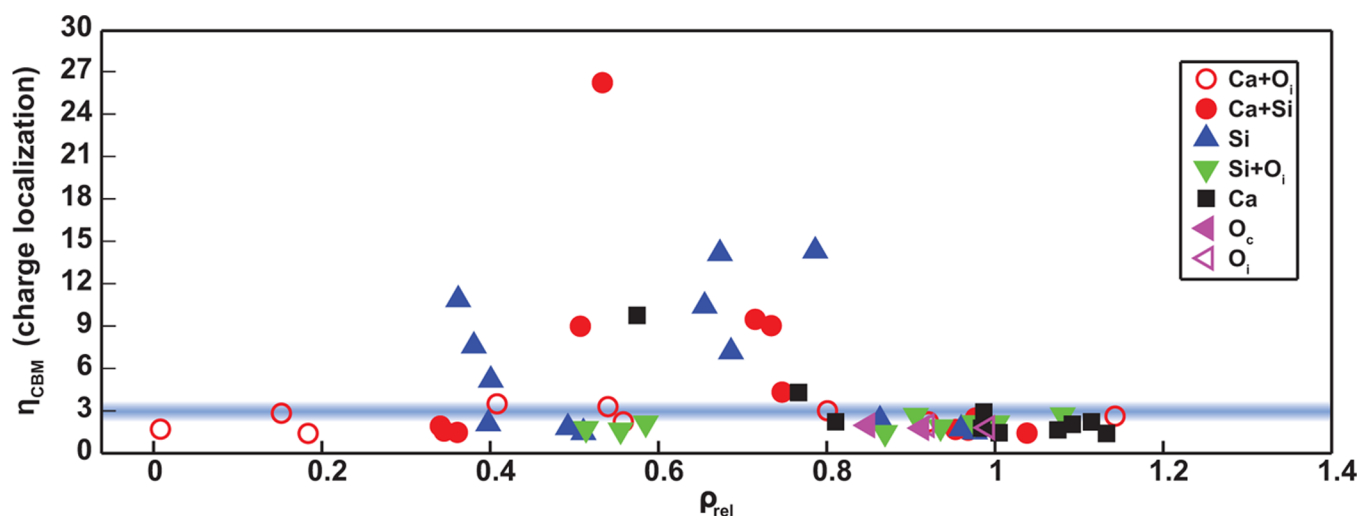


**Figure 4.** Charge localization over conduction band minimum ( $\eta_{\text{CBM}}$ ) versus charge transfer ratio, defined as  $\rho_{\text{rel}} = \Delta\rho_{\text{impurity}}/\Delta\rho_{\text{reference}}$  where  $\Delta\rho_{\text{impurity}}$  and  $\Delta\rho_{\text{reference}}$  are the absolute amount of charge transferred from the impurity to the rest of the system and the amount of charge transferred from the substituted atoms in the reference structure, respectively. The types of substitutions are indicated in the upper right legend. Again,  $\text{O}_i$  indicates ionically bonded and  $\text{O}_c$  indicates covalently bonded oxygen substitutions in pure  $\text{C}_3\text{S}$ .

oxygen sites in the case of single oxygen substitutions for the sake of completeness and comparison. The full set of impurities that have been investigated is shown in Figure 3.

Differences in charge transfer between the reference atoms in  $\text{C}_3\text{S}$  and the impurities in doped  $\text{C}_3\text{S}$  can give rise to the formation of hybridized states and charge localization on the impurity atom site as discussed in detail for Mg, Al, and Fe substitutions. In these cases where strong charge localization occurs for either the  $\rho_{\text{VBM}}$  or  $\rho_{\text{CBM}}$ , the maximum value of the charge density (MCD) at the corresponding bands will also increase. Charge will be concentrated in a smaller region, mostly on the impurity and neighboring atoms. Therefore, in order to quantify the charge localization,  $\eta$ , we introduce a

charge localization function such that  $\eta = \text{MCD}_{\text{doped}}/\text{MCD}_{\text{pure}}$  where  $\eta$  values close to 1 mean that there is no or weak additional charge localization compared to pure  $\text{C}_3\text{S}$ . In Figure 3, we show the localization of  $\rho_{\text{CBM}}$  in the  $\text{C}_3\text{S}$  structure with a range of substitutions. We can see from these results that  $\eta_{\text{CBM}}$  for Fe substitution is found to be the highest among all substitution cases considered. This analysis also identifies several other impurities such as As, In, Sn, Ge, Cd, and Hg, as some of the strongest substitution candidates that may localize charge in  $\text{C}_3\text{S}$ . Similar to Fe, these substitutions also heavily localize  $\rho_{\text{CBM}}$ , but differently they remain insulating despite a decrease in their band gaps to 2–2.5 eV from 3.98 eV for pure  $\text{C}_3\text{S}$ . We have also investigated  $\eta_{\text{VBM}}$  to see how  $\text{C}_3\text{S}$  changes

with substitutions when there is electrophilic chemical attack: however, we conclude that except for Fe there is no substitution that modifies  $\rho_{\text{VBM}}$  significantly. Inclusion of substitutions leads to the generation of hybridized states around the conduction band but not a significant change around the valence band. For this reason, we conclude that  $\eta_{\text{VBM}}$  does not change drastically upon substitution.

Thus far, we have discussed how charge transfer and charge localization are closely related. In order to quantify the degree of charge transfer between the reference  $\text{C}_3\text{S}$  and doped  $\text{C}_3\text{S}$  structures, we define a parameter  $\rho_{\text{rel}} = \Delta\rho_{\text{impurity}}/\Delta\rho_{\text{reference}}$  such that  $\rho_{\text{rel}}$  corresponds to the absolute amount of charge transferred from the impurity to the rest of the system,  $\Delta\rho_{\text{impurity}}$  divided by the amount of charge that was transferred from the substituted atoms in the reference structure,  $\Delta\rho_{\text{reference}}$ . This new parameter,  $\rho_{\text{rel}}$ , plotted in Figure 4 vs  $\eta$ , is useful to understand the relation between the localization of the charge and degree of the charge transfer itself upon substitution. We observe that near the region where  $\rho_{\text{rel}}$  is  $\sim 1$  significant charge localization is not expected. Our charge transfer and PDOS analysis for Mg, Al, and Fe in Figures 1 and 2 showed that charge donation imbalance between atoms that are substituted changes the characteristics of the conduction band and therefore causes charge localization. In the  $\rho_{\text{rel}} \approx 1$  case the substitute atom has almost the same chemical characteristics as the substituted atom in pure  $\text{C}_3\text{S}$  in terms of charge donation to the system. However, for substitutions with  $\rho_{\text{rel}}$  smaller than 0.8, we start to see a sudden increase in charge localization values for some of the impurities. In this case, the impurity atom holds its charge rather than transferring it to the system, therefore causing charge localization.

In addition to modification of the charge density in the conduction and valence bands, the structural reorganization upon doping yields several trends which also support the charge localization discussion. At the Si site, substitutions with groups IIIA, IVA, and VA atoms, which increase the size of the oxygen tetrahedra in  $\text{C}_3\text{S}$ , are also found to localize the charge on the impurity atom. The atomic radii of impurities at the center of the oxygen tetrahedra in  $\text{C}_3\text{S}$ ,  $a_{\text{impurity}}$ , become larger as we move down in the periodic table, such that  $a_{\text{In}} > a_{\text{Ga}} > a_{\text{Al}} > a_{\text{As}} > a_{\text{P}} > a_{\text{N}}$ , and  $a_{\text{Sn}} > a_{\text{Ge}} > a_{\text{Si}}$ . For that reason, as the distance between the impurity atom and the surrounding oxygens increases, the bonding between them will weaken, and the impurity atoms will donate less charge to the surrounding oxygen atoms. At the Ca site, there is no definite trend between atomic radii and charge localization for all substitutions in general. In the cases with strong charge localization, the nearest-neighbor distance between the impurity and surrounding O atoms is increased. The lack of such a trend for the case of the Ca substitution (as compared with Si) may be due to the fact that the Ca–O nearest-neighbor distance is longer compared to the Si–O distance in pure  $\text{C}_3\text{S}$  and that the orientation of oxygens around the Ca site is less ordered in comparison to the Si site. This argument also supports our preliminary tests in the M1 polymorph of the  $\text{C}_3\text{S}$  phase, where the results we have are very similar to our results in the M3 polymorph.  $\text{C}_3\text{S}$  polymorphs are known to be formed by displacive transformations, and the main difference that lies between these two polymorphs is the relative orientation of silicon tetrahedra.<sup>30</sup> Therefore, substitutions of different impurities are expected to provide similar environments.

Although our work attempts to shed light on the chemical interactions between substitutions in the  $\text{C}_3\text{S}$  phase from a

fundamental point of view, as we mentioned additional effects regarding kinetics of the reactions will also play an important role for determining the hydration reactivity.<sup>31,32</sup> Surface reconstruction, solvent effects, and fabrication techniques should also be considered in future studies.

## CONCLUSIONS

We employ density functional theory to analyze the effects of a range of impurities on tricalcium silicate ( $\text{C}_3\text{S}$ ) phases. We discuss the fundamental relation between charge localization of the impurities and charge transfer at the substitution site. We show that bulk substitutions strongly modify the conduction band minimum by hybridizing with surrounding oxygen atoms, therefore localizing reactive sites on select impurity atoms. Our calculations identify several impurities that can reduce the number of reactive sites throughout the material, and good agreement with the available experimental data is demonstrated.

## ASSOCIATED CONTENT

### Supporting Information

Relative charge transfer ( $\rho_{\text{rel}}$ ) and charge localization parameters of the CBM ( $\eta_{\text{CBM}}$ ) for all impurities in  $\text{C}_3\text{S}$  considered in this work;  $\eta_{\text{CBM}}$  vs  $\rho_{\text{rel}}$  figures are shown. This material is available free of charge via the Internet at <http://pubs.acs.org>.

## AUTHOR INFORMATION

### Corresponding Authors

\*E-mail: [kayahan@mit.edu](mailto:kayahan@mit.edu)

\*E-mail: [jcg@mit.edu](mailto:jcg@mit.edu)

### Notes

The authors declare no competing financial interest.

## ACKNOWLEDGMENTS

This work has been supported by the Concrete Sustainability Hub at MIT, with sponsorship provided by the Portland Cement Association (PCA). Calculations were performed in part at the National Energy Research Scientific Computing Center, which is supported by the Office of Science of the U.S. Department of Energy and in part by the National Science Foundation through Teragrid resources provided by TACC.

## REFERENCES

- (1) Taylor, H. *Cement Chemistry*, 2nd ed.; Thomas Telford Publishing: London, 1997.
- (2) Lea, F. M.; Hewlett, P. C. *Lea's Cement Chemistry of Cement and Concrete*, 4th ed.; Arnold: California, 2003.
- (3) Durgun, E.; Manzano, H.; Pellenq, R. J. M.; Grossman, J. C. Understanding and Controlling the Reactivity of the Calcium Silicate phases from First Principles. *Chem. Mater.* **2012**, *24*, 1262–1267.
- (4) Manzano, H.; Durgun, E.; Abdolhosseine Qomi, M. J.; Ulm, F.-J.; Pellenq, R. J. M.; Grossman, J. C. Impact of Chemical Impurities on the Crystalline Cement Clinker Phases Determined by Atomistic Simulations. *Cryst. Growth Des.* **2011**, *11*, 2964–2972.
- (5) Bullard, J. W.; Jennings, H. M.; Livingston, R. a.; Nonat, A.; Scherer, G. W.; Schweitzer, J. S.; Scrivener, K. L.; Thomas, J. J. Mechanisms of Cement Hydration. *Cem. Concr. Res.* **2011**, *41*, 1208–1223.
- (6) Cheung, J.; Jeknavorian, a.; Roberts, L.; Silva, D. Impact of Admixtures on the Hydration Kinetics of Portland Cement. *Cem. Concr. Res.* **2011**, *41*, 1289–1309.

- (7) Van Vliet, K.; Pellenq, R.; Buehler, M. J.; Grossman, J. C.; Jennings, H.; Ulm, F.-J.; Yip, S. Set in Stone? A Perspective on the Concrete Sustainability Challenge. *MRS Bull.* **2012**, *37*, 395–402.
- (8) de Queiroz Lamas, W.; Palau, J. C. F.; de Camargo, J. R. Waste Materials Co-processing in Cement Industry: Ecological Efficiency of Waste Reuse. *Renewable Sustainable Energy Rev.* **2013**, *19*, 200–207.
- (9) Bhatti, J. Role of Minor Elements in Cement Manufacture and Use. *Res. Dev. Bull. - Portland Cem. Assoc.* **1995**, 1–38.
- (10) Stark, J. Recent Advances in the Field of Cement Hydration and Microstructure Analysis. *Cem. Concr. Res.* **2011**, *41*, 666–678.
- (11) Hohenberg, P.; Kohn, W. Inhomogeneous Electron Gas. *Phys. Rev.* **1964**, *155*, B864–B871.
- (12) Kohn, W.; Sham, L. Self-consistent Equations Including Exchange and Correlation Effects. *Phys. Rev.* **1965**, *385*, A1697–A1705.
- (13) Blochl, P. Projector Augmented-wave Method. *Phys. Rev. B* **1994**, *50*, 17953–17979.
- (14) Kresse, G.; Hafner, J. Ab-Initio Molecular Dynamics for Liquid Metals. *Phys. Rev. B* **1993**, *47*, 558–561.
- (15) Kresse, G.; Furthmüller, J. Efficiency of Ab-initio Total Energy Calculations for Metals and Semiconductors Using a Plane-wave Basis Set. *Comput. Mater. Sci.* **1996**, *6*, 15–50.
- (16) Perdew, J.; Burke, K.; Ernzerhof, M. Generalized Gradient Approximation Made Simple. *Phys. Rev. Lett.* **1996**, *77*, 3865–3868.
- (17) Bader, R. F. W. A Quantum Theory of Molecular Structure and its Applications. *Chem. Rev.* **1991**, *91*, 893–928.
- (18) Tang, W.; Sanville, E.; Henkelman, G. A Grid-based Bader Analysis Algorithm without Lattice Bias. *J. Phys.: Condens. Matter* **2009**, *21*, 084204–084210.
- (19) de Noirfontaine, M.-N.; Dunstetter, F.; Courtial, M.; Gasecki, G.; Signes-Frehel, M. Polymorphism of Tricalcium Silicate, the Major Compound of Portland Cement Clinker. *Cem. Concr. Res.* **2006**, *36*, 54–64.
- (20) Parr, R. G.; Yang, W. Density Functional Approach to the Frontier-electron Theory of Chemical Reactivity. *J. Am. Chem. Soc.* **1984**, *106*, 4049–4050.
- (21) Chattaraj, P. K. *Chemical Reactivity Theory: A Density Functional View*; Taylor & Francis: U.K., 2009.
- (22) Geerlings, P.; De Proft, F.; Langenaeker, W. Conceptual Density Functional Theory. *Chem. Rev.* **2003**, *103*, 1793–1874.
- (23) Since charge densities are projected on single bands and calculated structures have no singularity, integrated charge density over the unit cell is  $2 e^-$  for all structures. Isosurface values for the band decomposed charge densities are 0.001.
- (24) Manzano, H.; Dolado, J. S.; Ayuela, A. Structural, Mechanical, and Reactivity Properties of Tricalcium Aluminate Using First-Principles Calculations. *J. Am. Ceram. Soc.* **2009**, *92*, 897–902.
- (25) Nicoleau, L.; Schreiner, E.; Nonat, A. Ion-specific Effects Influencing the Dissolution of Tricalcium Silicate. *Cem. Concr. Res.* **2014**, *59*, 118–138.
- (26) Odler, I.; Schüppstuhl, J. Early Hydration of Tricalcium Silicate III. Control of the Induction Period. *Cem. Concr. Res.* **1981**, *11*, 765–774.
- (27) Stephan, D.; Wistuba, S. Crystal Structure Refinement and Hydration Behaviour of  $3\text{CaO} \cdot \text{SiO}_2$  Solid Solutions with  $\text{MgO}$ ,  $\text{Al}_2\text{O}_3$  and  $\text{Fe}_2\text{O}_3$ . *J. Eur. Ceram. Soc.* **2006**, *26*, 141–148.
- (28) Thompson, R. A.; Killoh, D. C.; A, F. J. Crystal Chemistry and Reactivity of the MgO Stabilized Alites. *J. Am. Ceram. Soc.* **1975**, *58*, 54–57.
- (29) Kim, Y.-M.; Hong, S.-H. Influence of Minor Ions on the Stability and Hydration Rates of  $\beta$ -Dicalcium Silicate. *J. Am. Ceram. Soc.* **2004**, *87*, 900–905.
- (30) Dunstetter, F.; de Noirfontaine, M.-N.; Courtial, M. Polymorphism of Tricalcium Silicate, the Major Compound of Portland Cement Clinker. *Cem. Concr. Res.* **2006**, *36*, 39–53.
- (31) Mishra, R. K.; Flatt, R. J.; Heinz, H. Force Field for Tricalcium Silicate and Insight into Nanoscale Properties: Cleavage, Initial Hydration, and Adsorption of Organic Molecules. *J. Phys. Chem. C* **2013**, *117*, 10417–10432.
- (32) Manzano, H.; Pellenq, R. J. M.; Ulm, F.-J.; Buehler, M. J.; van Duin, A. C. T. Hydration of Calcium Oxide Surface Predicted by Reactive Force Field Molecular Dynamics. *Langmuir* **2012**, *28*, 4187–4197.